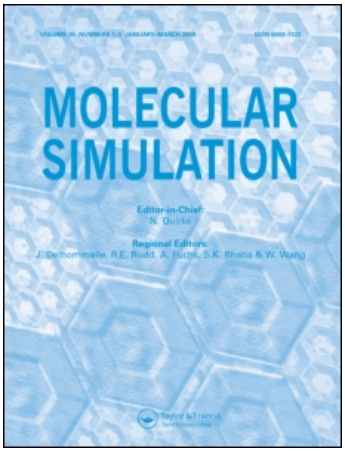

Molecular Simulation
Publication details, including instructions for authors and subscription information:
http://www.informaworld.com/smpp/title~content=t713644482

Molecular dynamics simulations of temperature- and pressure-induced solid-solid phase transitions in crystalline *para*-terphenyl

Bohdan Schatschneider[a]; Eric L. Chronister[a]
[a] Department of Chemistry, University of California, Riverside, CA, USA

To cite this Article Schatschneider, Bohdan and Chronister, Eric L.(2008) 'Molecular dynamics simulations of temperature- and pressure-induced solid-solid phase transitions in crystalline *para*-terphenyl', Molecular Simulation, 34: 10, 1159 — 1166
To link to this Article: DOI: 10.1080/08927020802411729
URL: http://dx.doi.org/10.1080/08927020802411729

Molecular Simulation
Vol. 34, Nos. 10–15, September–December 2008, 1159–1166

Taylor & Francis
Taylor & Francis Group

Molecular dynamics simulations of temperature- and pressure-induced solid–solid phase transitions in crystalline *para*-terphenyl

Bohdan Schatschneider and Eric L. Chronister*

Department of Chemistry, University of California, Riverside, CA, USA

(*Received 5 February 2008; final version received 12 August 2008*)

Molecular dynamics (MD) simulations of pressure- and temperature-induced solid–solid phase transitions in *para*-terphenyl have been investigated using Material Studio®. Initial simulations were performed using the COMPASS (condensed-phase optimised molecular potentials for atomistic simulation studies) force field to evaluate its ability to model the known temperature and pressure phase boundary between the triclinic and monoclinic crystal phases. Geometry optimisation using the universal COMPASS force field could not adequately model the experimental crystal structure at 113 K, and MD simulations could not adequately reproduce the known transition temperature at ambient pressure, nor yield a well-defined transition pressure at low temperature. However, a one-parameter optimisation of the torsion potential component of the polymer-consistent force field (PCFF) (incorporating COMPASS non-bond parameters) yielded MD simulations that accurately modelled the pressure–temperature boundary between the low-temperature low-pressure triclinic phase and the high-pressure high-temperature monoclinic phase of *para*-terphenyl.

Keywords: phase transition; solid–solid; *p*-terphenyl

1. Introduction

The solid–solid phase transitions in *para*-terphenyl (*p*TP) involve a competition between intermolecular packing forces that favour a planar molecular conformation and intramolecular *ortho*-hydrogen repulsion that favours torsion of the central phenyl ring. This competition gives rise to an order–disorder transition in *p*-terphenyl and the incommensurate phase transitions of other linear polyphenyl systems. Biphenyl, *p*-terphenyl and *p*-quaterphenyl all have monoclinic crystal structures at room temperature, with two molecules per unit cell. Although the molecules are flat on average, they have large librational motion about the long molecular axis coupled with torsional motion of adjacent phenyl rings through the mean molecular plane. One of the challenges of simulating the *p*TP phase boundary is accurately modelling the temperature-induced order–disorder transition (associated with phenyl ring motion on the torsional double-well potential) at ambient pressure, as well as the pressure-induced displacive transition at low temperature (where increased intermolecular interactions favour molecular planarity). The strong coupling of internal and external degrees of freedom make simulations of temperature- and pressure-induced phase transitions in *p*TP particularly challenging.

The low-temperature crystal structure of *p*TP at ambient pressure has a triclinic space group ($P\bar{1}$, $Z = 4$) with four inequivalent sites, each characterised by a unique torsion angle of the central phenyl ring [1,2]. At higher temperature and ambient pressure ($T_c = 193$ K, $P = 1$ atm) [2], an order–disorder phase transition occurs to a monoclinic ($P2_1/a$, $Z = 2$) space group [3] in which the average structure of the molecule is planar. The transition temperature for the order–disorder phase change decreases at higher pressure [4–7], as illustrated in Figure 1. At very low temperature, the phase transition becomes more displacive in character ($P_c \sim 5$–6 kbar, at $T = 0$ K) [8]. Less well characterised is the existence of other structural phases identified by inelastic neutron scattering (with a triple point at $T \sim 71$ K, $P = 3.5$ kbar [8]), and spectroscopic measurements at lower temperatures near the triclinic–monoclinic phase boundary [6,7]. The triclinic and monoclinic crystal structures are illustrated in Figure 2.

The well-developed experimental database for *p*TP under various temperature and pressure conditions makes it an excellent system with which to probe the fidelity of computational models. Crystal structures have been determined above and below the triclinic–monoclinic phase boundary by single-crystal X-ray measurements [1,9,10] and pressure-dependent powder X-ray diffraction measurements have characterised pressure-induced structural changes at ambient temperature [11,12]. The triclinic–monoclinic phase transition temperature (at ambient pressure) has been determine to be $T_c = 193$ K by scanning calorimetry [3,13]. Temperature- and pressure-dependent vibrational studies (e.g. infrared [14–17], Raman [18–20] and inelastic neutron scattering

*Corresponding author. Email: eric.chronister@ucr.edu

ISSN 0892-7022 print/ISSN 1029-0435 online

DOI: 10.1080/08927020802411729
http://www.informaworld.com

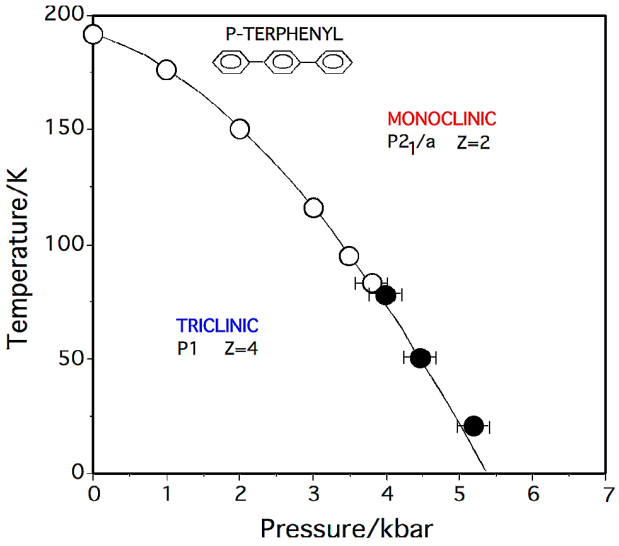

Figure 1. The pressure–temperature phase diagram for crystalline *para*-terphenyl [4,6,7]. The open circles are from low-frequency Raman measurements [5], and the solid circles are obtained from impurity spectra [6]. The solid line indicates the triclinic–monoclinic crystal phase boundary.

[21]) have revealed unique dynamics, including soft modes associated with the polymorphic phase transition. Inelastic neutron scattering [4,8,22] studies have also revealed evidence for a secondary higher pressure triclinic phase.

Previous molecular simulation studies have probed the correlation between the intermolecular rotational dynamics of the central phenyl ring of *p*TP and the corresponding changes in the crystal structure. Bordat and Brown [23] performed simulations of the temperature-induced triclinic–monoclinic phase transition of *p*TP using an optimised empirical potential with the DL_POLY MD suite to model the dynamics of $2 \times 2 \times 2$ pseudo-monoclinic cells (64 molecules). An empirical potential was used, which included a Buckingham (6-exp) potential, electrostatic interactions and an optimised intramolecular torsion potential [24–26]. Optimisation of the torsion potential (with a four-term Fourier series), as well as the optimisation of the CC and HH Buckingham potentials yielded a model that reproduced the crystal structure above and below the disorder–order (i.e. triclinic–monoclinic) transition temperature at ambient pressure [23]. Extensions of this work have included some pressure-dependent simulations at 150 K and the simulations of the dynamics of domain walls in the low-temperature phase [27]. A constrained MD simulation performed below the order–disorder transition temperature concluded that a critical torsion potential was required in order to observe a phase transition [28]. Monte Carlo (MC) simulations have also been used to model pressure-dependent changes within the monoclinic phase at room temperature [29].

Ab initio [30] and lattice dynamics [31] calculations have provided insight into pressure-induced changes in the electronic and vibrational properties of *p*TP. In particular, *ab initio* studies concluded that purely dispersive interactions are inadequate for modelling oligo-*para*-phenylenes due to the overlap of wave functions between the neighbouring molecules and the significant intermolecular band dispersion. In addition, pressure-dependent lattice dynamics calculations (in a self-consistent phonon approximation) have identified phonon instabilities (i.e. zero frequency at non-zero wave vector) associated with the order–disorder phase transition [31].

In the present study, MD simulations of *p*TP were performed to quantitatively model both the temperature-induced order–disorder solid–solid phase transition at ambient pressure and the pressure-induced displacive phase transition at low temperature. Initial simulations were performed utilising the universal condensed-phase force fields COMPASS (condensed-phase optimised molecular potentials for atomistic simulation studies) and PCFF (polymer-consistent force field). The COMPASS force field has been parameterised using condensed-phase properties as well as *ab initio* calculations and empirical data for isolated molecules [32]. This force field

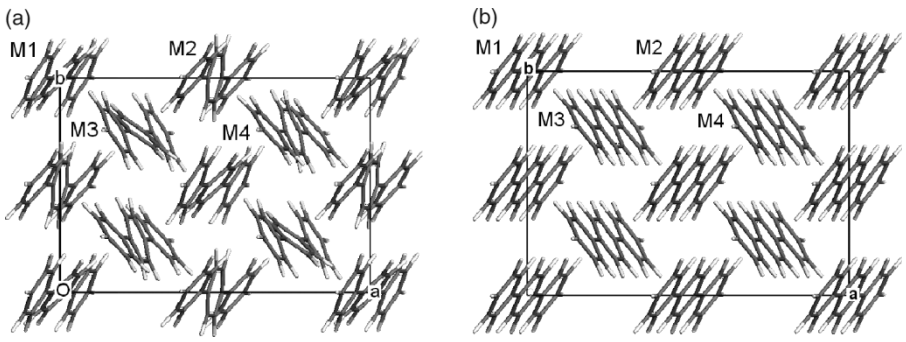

Figure 2. (a) Triclinic (pseudo-monoclinic) unit cell corresponding to $T = 113$ K and ambient pressure (viewed down the *c*-axis) [1]. (b) Monoclinic crystal structure (expanded $2 \times 2 \times 1$ cell) at room temperature and ambient pressure [9].

has been designed for accurate prediction of structural, conformational, vibrational and thermophysical properties for a broad range of molecules in condensed phases, and under a wide range of conditions of temperature and pressure [33–35]. Simulations were performed to evaluate the ability of these universal force fields to model the temperature and pressure phase boundary between the triclinic and monoclinic crystal phases of *p*TP. These generalised force fields have proved reasonably successful in reproducing molecular crystal structure parameters as well as temperature-induced changes in state [32]. However, simulations of *p*TP using COMPASS and PCFF proved unable to adequately model either the temperature or pressure-induced solid–solid phase transitions. The intramolecular torsion potential in PCFF is coupled to non-bond terms in the intermolecular potential, so a relatively minor one-parameter optimisation of the torsion potential (including non-bond parameters from COMPASS) yielded an improved potential that was able to accurately model the boundary between the low-temperature low-pressure triclinic phase and the high-pressure high-temperature monoclinic phase.

2. Methods

2.1 Computers

The MD simulations were performed using Accelrys Material Studio® 3.0–4.2. Calculations were performed on a Dell Pentium IV single-core 32-bit processor machine (2.59 GHz), Dell Pentium D duo-core 32-bit machine (3.19 GHz) and Dell quad-core Opteron 64-bit Linux machine (1.87 GHz).

2.2 Molecular dynamics simulations

The MD simulations were performed using the Discover hybrid Monte Carlo dynamics module of the Materials Studio computational suite. Discover implements classical mechanics using the Verlet integrator [36], an ABM4 (Adams–Bashforth–Moulton fourth order) algorithm as a predictor/corrector method (Accelrys Help Page: Equations of Motion) to propagate the dynamics and the Runge–Kutta method to initiate the process. An NPT statistical ensemble was used with a 'Berendsen thermostat' [37] and a 'Parrinello barostat' [29] (Parrinello–Rahman variable shape simulation). An atom-based summation method was used with adjustable site–site cut-off parameters from 9.5 to 15 Å for the non-bond interactions. Simulations were performed with 1 fs steps, sampled every 100 steps, without any symmetry restrictions.

The starting configurations of *p*TP for all simulations was taken as either the 113 K triclinic (pseudo-monoclinic) structure from Baudour et al. [1] (Figure 2(a)) or the room-temperature monoclinic structure from Rietveld et al. [9] (Figure 2(b)). The torsion angles for the four inequivalent sites corresponding to the four inequivalent molecular sites M_1, M_2, M_3 and M_4 in the triclinic structure have four unique torsion angles, $t_1 = 15.30°$, $t_2 = -26.90°$, $t_3 = -23.38°$ and $t_4 = 18.30°$. The torsion coordinate is illustrated in Figure 3. By contrast, all of the molecules in the monoclinic phase are close to planar on average. Therefore, the internal torsion angle of the molecules is a relevant coordinate for characterising the triclinic–monoclinic phase transition of *p*TP [23].

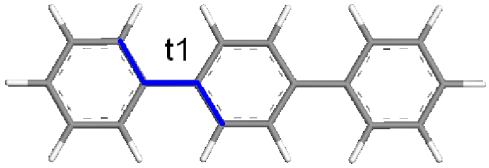

Figure 3. *para*-Terphenyl molecule with torsion angle t_1 corresponding to a molecule in crystallographic site M_1.

2.3 Force fields

The COMPASS and PCFF force fields provided with Materials Studio were evaluated for their ability to model the solid–solid triclinic–monoclinic phase transition of *p*TP. COMPASS has been optimised for condensed-phase simulations and is based on earlier CFF9x and PCFF force fields [32]. A number of studies have been performed [33,34] using COMPASS to model molecular structures, vibrational frequencies and liquid PVT behaviour. COMPASS has also been utilised to obtain crystal structures, lattice energies, heats of vaporisation and solubility parameters [35].

The functional form of the COMPASS and PCFF force fields can be expressed as the sum of three energetic terms, $\boldsymbol{E}_{\text{total}} = \boldsymbol{E}_{\text{internal}} + \boldsymbol{E}_{\text{coupling}} + \boldsymbol{E}_{\text{intramolecular}}$, defined below [32,38]:

$$\begin{aligned} E_{\text{internal}} = &\sum_b [k_{2b}(b-b_0)^2 + k_{3b}(b-b_0)^3 + k_{4b}(b-b_0)^4] \\ &+ \sum_\theta [k_{2\theta}(\theta-\theta_0)^2 + k_{3\theta}(\theta-\theta_0)^3 \\ &+ k_{4\theta}(\theta-\theta_0)^4] + \sum_\phi [V_1(1-\cos\phi) \\ &+ V_2(1-\cos 2\phi) + V_3(1-\cos 3\phi)] + \sum_\chi k_{2\chi}\chi^2. \end{aligned} \tag{1a}$$

The internal valence coordinates are bond stretch (b), angle (θ), torsion angle (ϕ) and out-of-plane angle (χ). Internal coupling terms are also important for determining

structural variations and vibrational frequencies

$$\begin{aligned} E_{\text{coupling}} = & \sum_{b,b'}[k_{bb'}(b-b_0)(b'-b'_0)] \\ & + \sum_{b,\theta}[k_{b\theta}(b-b_0)(\theta-\theta_0)] \\ & + \sum_{b,\phi}[(b-b_0)(k_{1b\phi}\cos\phi + k_{2b\phi}\cos 2\phi \\ & + k_{3b\phi}\cos 3\phi)] \\ & + \sum_{\theta,\phi}[(\theta-\theta_0)(k_{1\theta\phi}\cos\phi \\ & + k_{2\theta\phi}\cos 2\phi + k_{3\theta\phi}\cos 3\phi)] \\ & + \sum_{\theta,\theta'}[k_{\theta\theta'}(\theta-\theta_0)(\theta'-\theta'_0)] \\ & + \sum_{\theta,\theta',\phi}[k_{\phi\theta\theta'}(\theta-\theta_0)(\theta'-\theta'_0)\cos\phi]. \end{aligned} \tag{1b}$$

The intramolecular non-bonding interactions are described by a sum of Leonard-Jones-9-6 van der Waals interactions plus Coulombic electrostatic interactions

$$E_{\text{intramolecular}} = \sum_{i,j}\frac{q_i q_j}{r_{ij}} + \sum_{i,j}\varepsilon_{ij}\left[2\left(\frac{r^0_{ij}}{r_{ij}}\right)^9 - 3\left(\frac{r^0_{ij}}{r_{ij}}\right)^6\right], \tag{1c}$$

where q_i is the partial charge on atom i and r_{ij} is the distance separating atoms. To make the partial charge parameters transferable, they are expressed as a sum of charges associated with each bond. Similarly, the LJ-9-6 parameters r_i^0 and ε_i are only defined for like 'i' atom pairs and off-diagonal mixed atom interactions are parameterised as [39]

$$r^0_{ij} = \left(\frac{\left(r^0_i\right)^6 + \left(r^0_j\right)^6}{2}\right)^{1/6}$$
$$\varepsilon_{ij} = 2\sqrt{\varepsilon_i \cdot \varepsilon_j}\left(\frac{\left(r^0_i\right)^3 \cdot \left(r^0_j\right)^3}{\left(r^0_i\right)^6 \cdot \left(r^0_j\right)^6}\right). \tag{2}$$

In the present study, MD simulations were performed using COMPASS, PCFF and an optimised PCFF potential was evaluated, which incorporates the COMPASS van der Waals parameters and varies only the second-order intramolecular torsion potential term V_2.

3. Results

3.1 *Optimising a force field for* para-*terphenyl*

Calculated crystallographic parameters are listed along with experimental X-ray data (at 113 K [2]) in Table 1. Two of the three unit cell angles in the triclinic phase ($Z = 4$) are close to 90° and it is common to treat this phase as pseudo-monoclinic, with $\alpha = \gamma = 90°$ [2]. Table 1 shows that neither COMPASS nor PCFF can adequately model either the experimental unit cell parameters or the intramolecular torsion angles at $T = 113$ K. The universal COMPASS force field most likely does not adequately model the coupling of the intramolecular torsion potential with librational motion in condensed-phase oligo-*para*-phenylenes such as *p*TP. Both COMPASS and PCFF predict an ambient pressure triclinic–monoclinic phase transition temperature $T_c \sim 90$ K, and since this is well below the experimental value of $T_c = 193$ K [2], neither

Table 1. Experimental and simulated torsion angles and unit cell parameters at $T = 113$ K and $P = 1$ atm.

		Simulated torsion angles					
				PCFFC#			
Site	Experimental X-ray [2]	COMPASS	PCFF	2	4	6	7
M_1	15.2	1.6	1.02	26.3	24.3	19.4	13.4
M_2	−26.8	−0.9	−10.6	−28.8	−26.3	−22.1	−17.9
M_3	18.3	−6.0	2.04	24.5	22.9	20.7	18.2
M_4	−23.4	−2.6	−1.7	−27.4	−25.1	−23.0	−14.0
Cell parameters							
a (Å)	16.01	14.38	14.37	16.89	16.86	16.74	16.61
b (Å)	11.09	11.74	11.76	10.66	10.69	10.73	10.75
c (Å)	13.53	14.48	14.49	13.4	13.39	13.38	13.4
α	90.0°	90.0°	90.0°	90.6°	90.6°	90.6°	90.7°
β	92.0°	85.5°	90.0°	95.1°	95.4°	95.8°	95.7°
γ	90.0°	90.0°	85.7°	90.1°	90.0°	90.0°	89.6°

Simulation parameters: 50,000 steps, 9.5 Å non-bond cut-off, NPT, 64 molecules.

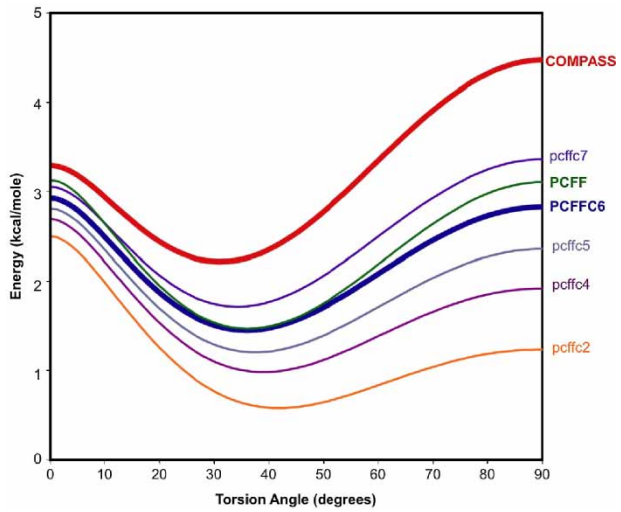

Figure 4. Torsion potential profiles as a function of the V_2 parameter torsion parameter listed in Table 2.

of these potentials reproduces the triclinic structure at 113 K. The deficiency in the COMPASS and PCFF force fields yields lattice constants that differ significantly ($\geq 10\%$) from experimental values, and yields an acute versus obtuse β angle [11]. The unique torsional dynamics of *p*TP requires optimisation of these generic force fields.

3.1.1 *Optimisation of the torsion potential*

Since COMPASS is not easily modified within Materials Studio, a minor optimisation of the PCFF condensed-phase force field was evaluated. Given the success of COMPASS in modelling other condensed-phase systems, the non-bond parameters from COMPASS were incorporated into PCFF (PCFFC) and the optimisation was limited to only one adjustable parameter, i.e. the second-order intramolecular torsion potential term, V_2, from Equation (1). Table 1 includes a comparison of experimental X-ray [2] and calculated unit cell parameters (and site-specific torsion angles) obtained using modified PCFFC force fields at 113 K. All of the modified PCFFC force fields yielded unit cell parameters that differed from experiment by 5%, with β angle a few degrees larger than the experimental value, e.g. ~95° versus 92°. The site-specific intramolecular torsion angles were more sensitive and could be reasonably tuned by adjusting only the V_2 torsion parameter. The modified force fields PCFFC2 and PCFFC4 yield torsion angles ~10° larger than experiment for sites M_1 and M_3, while PCFFC7 yielded torsion angles ~10° smaller than experiment for sites M_2 and M_4. The PCFFC6 force field provided the best correlation with the experimental unit cell parameters and also adequately modelled the site-specific intramolecular torsion angles.

The second-order V_2 torsion potential term and the non-bond parameters from COMPASS have a strong influence on the shape and barrier heights of the overall torsion potential, as shown in Figure 4. Table 2 lists the non-bond and torsion potential terms for the potential curves shown in Figure 4. The overall torsion potential for the COMPASS force field plotted in Figure 4 shows a relatively small 1.1 kcal/mol potential barrier at $\phi = 0°$ and a 2.3 kcal/mol barrier at $\phi = 90°$. Facile torsional rotation through the molecular plane using the COMPASS force field is consistent with erratic ring flips observed in MD simulations using the COMPASS force field (not shown).

To facilitate a comparison of the optimised PCFFC# force fields with previous *p*TP models [23], the minimum energy torsion angle ϕ_{min} and barrier heights at $\phi = 0°$ and 90° relative to the minimum torsional energy are included in Table 2. The comparison of different *p*TP torsion potentials [23,25,26] evaluated in [23] yielded ϕ_{min} values in the range 45–50°, with barrier heights in the range of $V(0°) = 2.6–3.5$ kcal/mol and $V(90°) = 1.4–2.0$ kcal/mol. The optimised potential reported in [23] had $\phi_{min} = 50°$, $V(0°) = 2.7$ kcal/mol and $V(90°) = 1.4$ kcal/mol. These parameters can be contrasted with the optimised PCFFC6 torsion potential for which $\phi_{min} = 36°$, with barrier heights of $V(0°) = 1.48$ kcal/mol and $V(90°) = 1.38$ kcal/mol. Both PCFFC6 and the optimised potential from [23] have similar barrier heights at $\phi = 90°$ and in both cases $V(\phi = 0°) > V(\phi = 90°)$. Although, $\phi_{min} = 36°$ for PCFFC6 is significantly lower than $\phi_{min} = 50°$ for the optimised potential in [23], it is similar

Table 2. Force field parameters for the torsion potential curves in Figure 4.

	Explicit torsion terms			Non-bond (LJ 6-9) terms				Relative torsion barriers		
	V_1	V_2	V_3	r_C^0	r_H^0	ε_C^0	ε_H^0	ϕ_{min}°	$V(\phi = 0°)$	$V(\phi = 90°)$
PCFF	8.3667	1.1932	0.0000	4.0100	2.9950	0.0640	0.0200	36	1.66	1.64
COMPASS	–	–	–	3.9150	2.8780	0.0680	0.0230	31	1.08	2.26
PCFFC2	8.3667	0.9000	0.0000	3.9150	2.8780	0.0680	0.0230	42	1.92	0.66
PCFFC4	8.3667	0.9600	0.0000	3.9150	2.8780	0.0680	0.0230	39	1.71	0.94
PCFFC5	8.3667	1.0000	0.0000	3.9150	2.8780	0.0680	0.0230	38	1.61	1.16
PCFFC6	8.3667	1.0432	0.0000	3.9150	2.8780	0.0680	0.0230	36	1.48	1.38
PCFFC7	8.3667	1.0932	0.0000	3.9150	2.8780	0.0680	0.0230	34	1.34	1.65

to the $\phi_{min} = 40^\circ$ associated with *ab initio* calculations on biphenyl [26]. The different non-bond interactions and the importance of steric hindrance to torsional dynamics in the crystal give rise to differences in the optimised torsional potentials. The PCFFC6 force field obtained by a one-parameter optimisation of a generic force field yields a generic potential suitable for modelling *p*TP and possibly other linear polyphenyl systems.

3.2 *Modelling the temperature-dependent order–disorder triclinic to monoclinic phase transition in* p*TP*

Temperature-dependent MD simulations of *p*TP at ambient pressure using the COMPASS force field yielded a triclinic–monoclinic phase transition temperature of only ~90 K, suggesting that the COMPASS torsion potential is inadequate for this system. Since the PCFFC6 force field adequately reproduced the average torsion angles for *p*TP at 113 K (with 64 molecules, 50,000 1 fs steps and a 10 Å cut-off), it was used for MD simulations of the temperature-dependent phase transition. The temperature dependence of the absolute value of the average dihedral torsion angles reveal a well-resolved phase transition near the experimental value of $T_c = 193$ K, as shown in Figure 5. The temperature-dependent curves also agree well with previous MD simulations using force fields optimised specifically for *p*TP [23].

Near the critical phase transition temperature large fluctuations were observed in the average torsion angle $\langle\phi\rangle$ obtained for different simulation runs. The fluctuation in $\langle\phi\rangle$ at temperatures near T_c were not reduced by longer simulation times. Simulation times of 50,000, 100,000 and 150,000 1 fs steps all yielded the same run-to-run fluctuations in $\langle\phi\rangle$ near T_c. The inability of increased MD simulation time to reduce run-to-run fluctuations in $\langle\phi\rangle$ indicates that the dynamics are very sensitive to initial velocities. By averaging several different simulation runs, these fluctuations averaged out. The temperature-dependent average torsion angles plotted in Figure 5 are the average of eight independent 150,000 step MD simulations of 64 molecules with a 15 Å cut-off using the PCFFC6 force field at ambient pressure.

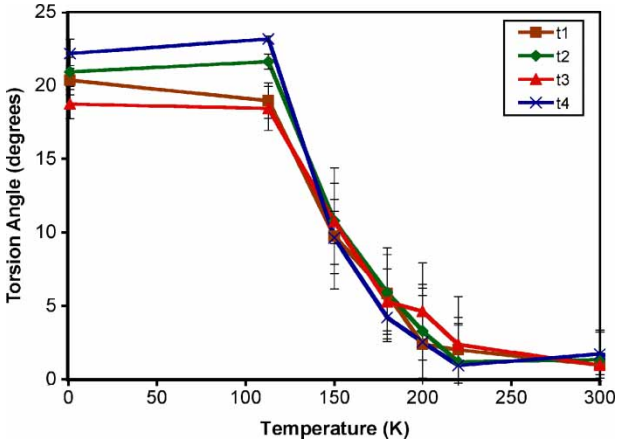

Figure 5. Variation in absolute value of the average dihedral angle as a function of temperature for MD simulations using the PCFFC6 force field.

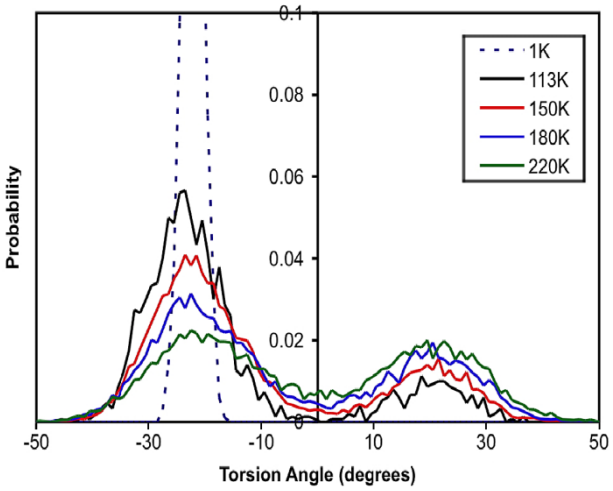

Figure 6. The t_2 dihedral angle distribution as a function of temperature using PCFFC6. The peak at $T = 1$ K is off-scale.

The raw t_2 dihedral angle distributions used to calculate the average torsion angles plotted in Figure 5 are shown in Figure 6. At extremely low temperatures, the torsion distribution has a narrow distribution since there is not enough energy to cross over the internal ring torsion barrier. With an increase in temperature, the narrow low-temperature distribution broadens to a bimodal distribution when the central ring can rotate over the torsional barrier associated with the molecular plane.

3.3 *Modelling the pressure-induced displacive triclinic–monoclinic phase transition at low temperature*

The COMPASS force field yielded unphysical pressure-dependent torsional dynamics in *p*TP (e.g. erratic flips in the sign of the torsion angle) reinforcing the need for an optimised potential. MD simulations were performed using the PCFFC6 force field at $T = 20$ K and at a variety of pressures in the range 0–0.5 GPa (64 molecules, 50,000 steps, 9.5 Å non-bond cut-off, 113 K triclinic starting structure). The resulting pressure-dependent average torsion angles and torsion angle distributions are shown in Figures 7 and 8, respectively. Figure 7 shows that the average torsion angle decreases dramatically at $P = 0.4$ GPa, indicative of a phase transition to the monoclinic crystal structure. Although the PCFFC6 force field successfully reproduced the pressure-induced displacive phase transition, the magnitude of the critical

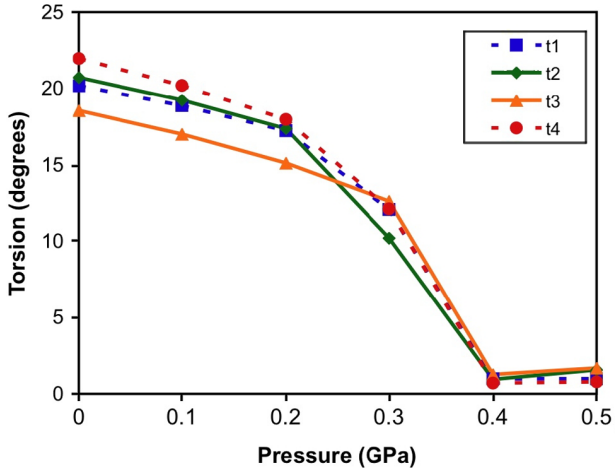

Figure 7. Pressure dependence of the average dihedral angle (absolute value) at $T = 20$ K using the PCFFC6 force field.

phase transition pressure $P_c \sim 0.4$ GPa is a little below the 0.5 GPa value expected from the phase diagram shown in Figure 1. Although further refinement of the PCFFC force field could improve the correlation between the simulated and experimental transition pressure, it is reassuring that a one-parameter optimisation of the PCFFC6 force field to reproduce the ambient pressure crystal structure at 113 K was sufficient to yield a reasonable model of the pressure-induced phase transition at low temperature.

It is relevant to note that the dihedral angle distributions shown in Figure 8 (for t_2, calculated using PCFFC6 at low temperature, $T = 20$ K) were unimodal and did not experience unphysical sign changes under pressure, in contrast to MD simulations performed with COMPASS (not shown). The torsion angle distributions in Figure 8 show that an increase in pressure causes the narrow unimodal t_2 angle distribution shift towards zero and broaden as the molecule becomes more planar.

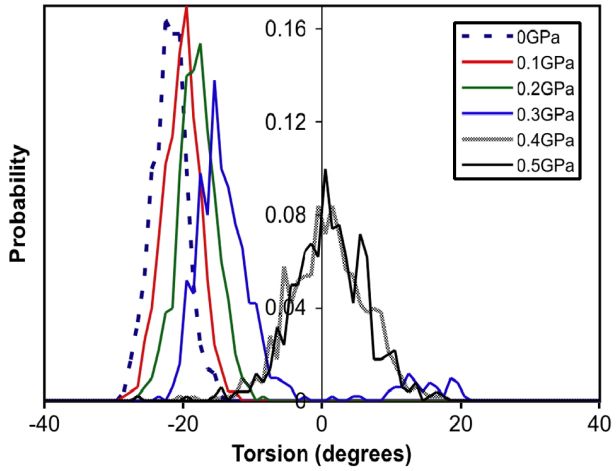

Figure 8. Pressure dependence of the t_2 torsion angle at $T = 20$ K using the PCFFC6 force field.

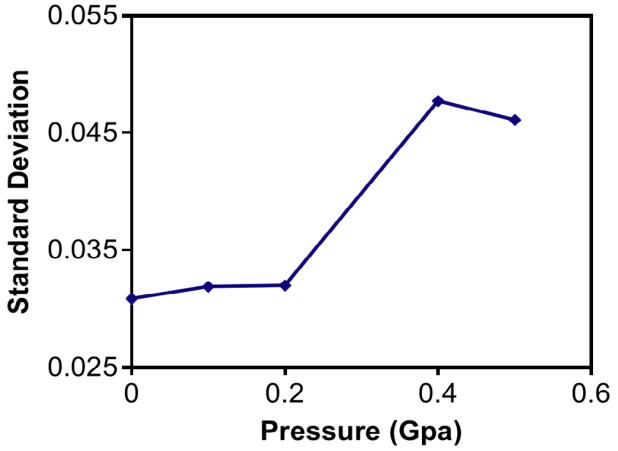

Figure 9. SD of the dihedral torsion angle distribution for t_2 as a function of pressure at $T = 20$ K.

3.4 Broadening of the torsion angle distribution near the phase transition pressure

As the system approaches the transition pressure P_c, the angular distributions shown in Figure 8 are observed to broaden. The magnitude of this broadening is shown by the pressure-dependent standard deviation (SD) of the distributions shown in Figure 9 (the width at 0.3 GPa is not included because of the slight bimodal nature to that distribution). The broadening of the distribution of torsion angles corresponds to increased fluctuations expected near the phase transition. The increased width of the distributions at the transition pressure is observed for all of the molecular sites in the crystal, indicating significant rearrangement of the crystal.

4. Conclusion

MD simulations using the COMPASS and PCFF universal force fields were found to be inadequate for modelling the solid–solid phase transition of *p*TP. However, a minor single-parameter modification of the generic PCFF torsion potential (including COMPASS non-bond terms) was found to quantitatively model both the temperature-induced order–disorder phase transition at ambient pressure and the pressure-induced displacive transition at low temperature. MD simulations reveal that the high-temperature monoclinic phase is characterised by a broad bimodal distribution of torsion angles with a correspondingly small average torsion angle. By contrast, the effect of high pressure at low temperature is to reduce the torsion angles associated with the four triclinic sites as the molecules flatten. MD simulations reveal that the high-temperature monoclinic phase is dynamically flat on average, while the high-pressure monoclinic phase is characterised by intrinsically small torsional angles. The increased width of the torsion angle distribution near the phase transition pressure also

suggests significant coupling between the intermolecular displacive transition and the intramolecular torsional degree of freedom. The nearly generic PCFFC6 potential makes simulations of *p*TP (and related linear *para*-phenylenes) accessible to a broader audience. However, modelling of the microscopic mechanisms of subtle effects such as the dynamics of domain walls or impurity molecules may require a more specialised potential.

Acknowledgements

This work was supported by the ACS Petroleum Research Fund (#37400-AC5) and the U.S. National Science Foundation (CHE-0612957).

References

[1] J.L. Baudour, Y. Delugeard, and H. Cailleau, *Structural transition in polyphenyls. I. Crystal structure of the low temperature phase of p-terphenyl at 113.deg.K*, Acta. Cryst. B32 (1976), pp. 150–154.

[2] J.L. Baudour, H. Cailleau, and W.B. Yellon, *Structural phase transition in polyphenyls. IV. Double-well potential in the disordered phase of p-terphenyl from neutron (200 K) and X-ray (room-temperature) diffraction data*, Acta. Cryst. B33 (1977), pp. 1773–1780.

[3] K. Saito, T. Atake, and H. Chihara, *Thermodynamic studies on order-disorder phase transitions of p-terphenyl and p-terphenyl-d14*, Bull. Chem. Soc. Jpn. 61 (1988), pp. 2327–2336.

[4] H. Cailleau, J.L. Baudour, J. Meinnel, A. Dworkin, F. Moussa, and C. Zeyen, *Double-well potentials and structural phase transitions in polyphenyls*, Faraday Discuss. Chem. Soc. 69 (1980), pp. 7–18.

[5] H. Cailleau, A. Girard, J.C. Messager, Y. Delugeard, and C. Vettier, *Influence of pressure on structural phase transitions in P-polyphenyls*, Ferroelectrics 54 (1984), pp. 257–260.

[6] E.L. Chronister and B. Baer, *Pressure induced phase transitions in pentacene doped para-terphenyl probed by changes in the impurity absorption spectrum*, J. Chem. Phys. 99 (1993), pp. 3137–3138.

[7] B. Baer and L. Chronister, *A high pressure optical study of dynamic and structural changes in pentacene doped para-terphenyl at low temperature*, High Press. Res. 12 (1994), pp. 101–110.

[8] B. Toudic, P. Launois, F. Moussa, A Girard, and H. Cailleau, *Pressure dependence of conformational instabilities in crystalline p-terphenyl*, Ferroelectrics 80 (1988), pp. 241–244.

[9] H.M. Rietveld, E.N. Maslen, and J. Clews, *An X-ray and neutron diffraction refinement of the structure of p-terphenyl*, Acta Cryst. B26 (1970), pp. 693–706.

[10] J.L. Baudour, L. Toupet, Y. Delugeard, and S. Ghemid, *Transitions de phase structurales dans les polyphenyles. IX. Affinements des structures du p-terphenyle hydrogens a 200 K (diffraction des rayons X) et du biphenyle deutere a 40 K (diffraction des neutrons)*, Acta Cryst. C42 (1986), pp. 1211–1217.

[11] G. Heimel, P. Puschnig, M. Oehzelt, K. Hummer, B. Koppelhuber-Bitschnau, F. Porsch, C. Ambrosch-Draxl, and R. Resel, *Chain-length-dependent intermolecular packing in polyphenylenes: a high pressure study*, J. Phys. Condens. Matter 15 (2003), pp. 3375–3389.

[12] P. Puschnig, G. Heimel, K. Weinmeier, R. Resel, and C. Ambrosch-Draxl, *High pressure studies on the optical and electronic properties of para-terphenyl*, High Press. Res. 22 (2002), pp. 105–109.

[13] H. Cailleau and A. Qworkin, *Calorimetric study of the phase transition of p-terphenyl*, Mol. Cryst. Liq. Cryst. 50 (1979), pp. 217–221.

[14] K.K. Zhuravlev and D. McCluskey, *Conformation of p-terphenyl under hydrostatic pressure*, J. Chem. Phys. 120 (2004), pp. 1841–1845.

[15] A. Ghanem, L. Bokobza, and C. Noel, *Conformational analysis of p-terphenyl by vibrational spectroscopy*, J. Molec. Struct. 159 (1987), pp. 47–63.

[16] M.B. Johnston, L.M. Herz, A.L.T. Khan, A. Kohler, A.G. Davies, and E.H. Linfield, *Low-energy vibrational modes in phenylene oligomers studied by THz time-domain spectroscopy*, Chem. Phys. Lett. 377 (2003), pp. 256–262.

[17] B. Schatschneider and E.L. Chronister, *High-resolution FTIR study of the para-terphenyl phase transition at high pressure*, J. Luminescence 127 (2007), pp. 34–40.

[18] A. Girard, H. Cailleau, Y. Marqueton, and C. Ecolivet, *Raman scattering study of the order-disorder phase transition in para-terphenyl*, Chem. Phys. Lett. 54 (1978), pp. 479–482.

[19] A. Girard, M. Sanquer, and Y. Delugeard, *Raman study of para-terphenyl:-influence of the isotopic substitution and interpretation of the spectra in both phases*, Chem. Phys. 96 (1985), pp. 427–434.

[20] A.M. Amorim da Costa, and A.M. Amado, *Doping effects in p-terphenyl molecular crystals: a study by Raman spectroscopy*, Solid State Ionics 125 (1999), pp. 263–269.

[21] P.A. Reynolds and W. White, *Inelastic neutron scattering spectrum of p-terphenyl*, J. Chem. Soc., Faraday Trans 68 (1972), pp. 1434–1438.

[22] B. Toudic, H. Cailleau, J. Gallier, and R.E. Lechner, *Local dynamics around structural order-disorder phase transitions*, J. Phys. (France) I 2 (1992), pp. 829–844.

[23] P. Bordat and R. Brown, *A molecular model of p-terphenyl and its disorder-order transition*, Chem. Phys. 246 (1999), pp. 323–334.

[24] A. Karpfen, C.H. Choi, and M. Kertesz, *Single-bond torsional potentials in conjugated systems: a comparison of* ab initio *and density functional results*, J. Phys. Chem. A 101 (1997), pp. 7426–7433.

[25] J.J.P. Stewart, *Mopac Manual* (6th ed.), Frank J. Seiler Research Laboratory, United States Air Force Academy, CO 80840, USA, 1990.

[26] S. Tsuzuki and K. Tanabe, Ab initio *molecular orbital calculatlons of the internal rotational potential of biphenyl using polarized basis sets with electron correlation correction*, J. Phys. Chem. 95 (1991), pp. 139–144.

[27] P. Bordat, A. Marbeuf, and R. Brown, *Molecular simulation of solid-solid phase transitions*, Mol. Sim. 32 (2006), pp. 971–984.

[28] A. Baranyai and T.R. Welberry, *Molecular dynamics simulation study of solid polyphenyls: structures determined by the interplay between intra- and intermolecular forces*, Mol. Phys. 75 (1992), pp. 867–879.

[29] N.A. Murugan and S. Yashonath, *Pressure induced orientational ordering in p-terphenyl*, J. Phys. Chem. B. 109 (2005), pp. 1433–1440.

[30] P. Puschnig, K. Hummer, and C. Ambrosch-Draxl, *Electronic, optical, and structural properties of oligophenylene molecular crystals under high pressure: an* ab initio *investigation*, Phys. Rev. B 67 (2003), 235321.

[31] T. Wasiutynski and H. Cailleau, *Lattice dynamics and structural instabilities of solid biphenyl and p-terphenyl-effect of pressure*, J. Phys. Condens. Matter 4 (1992), pp. 6241–6525.

[32] H.J. Sun, *COMPASS: An* ab initio *force-field optimized for condensed-phase applications overview with details on alkane and benzene compounds*, Phys. Chem. B102 (1998), pp. 7338–7364.

[33] H. Sun and D. Rigby, *Polysiloxanes:* ab initio *force field and structural, conformational and thermophysical properties*, Spectrochim. Acta A53 (1997), pp. 1301–1323.

[34] D. Rigby, H. Sun, and B.E. Eichinger, *Computer simulations of poly(ethylene oxide): force field, pvt diagram and cyclization behaviour*, Polym. Int. 44 (1997), pp. 311–330.

[35] T. Spyriouni and C. Vergelati, *A molecular modeling study of binary blend compatibility of polyamide6 and poly(vinyl acetate) with different degrees of hydrolysis: an atomistic and mesoscopic approach*, Macromolecules 34 (2001), pp. 5306–5316.

[36] L. Verlet, *Computer "experiments" on classical fluids. I. Thermodynamical properties of Lennard-Jones molecules*, Phys. Rev. 159 (1967), pp. 98–103.

[37] H.C. Andersen, *Molecular dynamics simulations at constant pressure and/or temperature*, J. Chem. Phys. 72 (1980), pp. 2384–2393.

[38] M.J. Hwang, T.P. Stockfisch, and A.T. Hagler, *Derivation of Class II force fields. 2. Derivation and characterization of a Class II force field, CFF93, for the alkyl functional group and alkane molecules*, J. Am. Chem. Soc. 116 (1994), pp. 2515–2525.

[39] M. Waldman and A.T.J. Hagler, *New combining rules for rare gas van der Waals parameters*, Comput. Chem. 14 (1993), pp. 1077–1084.